Proceedings of the Eighteenth International Conference on
Civil, Structural and Environmental Engineering Computing
Edited by: P. Iványi, J. Kruis and B.H.V. Topping
Civil-Comp Conferences, Volume 10, Paper 16.3
Civil-Comp Press, Edinburgh, United Kingdom, 2025
ISSN: 2753-3239, doi: 10.4203/ccc.10.16.3

Reformulating Peak Counting into a Circle Counting Approach to Enhance the Robustness of Automated Rebar Counting

S. T. Chun, J. S. Park and H. S. Park

Architectural Engineering, Yonsei University
seoul, South Korea

Abstract

Accurately ensuring the quantity of reinforcing bars before concrete pouring is critical for quality assurance in reinforced concrete structures. However, on-site rebar inspections are still carried out manually and restricted to a small number of sample areas, making them time-consuming and potentially unreliable. Consequently, such methods fall short in delivering reliable, and comprehensive quality assurance. To overcome these limitations, this study proposes a novel method for automatically counting rebars from grayscale-converted field images. The binary image in Cartesian coordinates is transformed into a polar coordinate system, such that vertical rebars appear as concentric circles. Instead of counting peaks from the vertical projection profile of rebar pixels in the binary image—as in conventional approaches—this method estimates the number of rebars by counting the number of circles. To enable accurate estimation of the number of concentric circles, we propose a radial transition voting algorithm. This algorithm performs a 360-degree scan from the image center and estimates the number of rebars by counting the intensity transitions along the radial direction in the binary image. This approach enables robust and fully automated rebar counting without the need for threshold tuning or parameter adjustment.

Keywords: automated rebar counting, polar transformation, radial-transition voting, image-to-image translation, projection profile, reinforced-concrete inspection.

1 Introduction

The structural performance and durability of reinforced concrete structures are highly dependent on the accurate on-site installation of reinforcing bars (rebars) according to the specified diameters, spacings, and quantities [1]. Current field inspections of rebar placement still rely on tape measurements and visual assessments, which are conducted over localized areas selectively sampled by inspectors. As a result of the limited and selectively inspected areas, this approach lacks the consistency and coverage required to ensure overall quality. It is also time-consuming and has been criticized for resulting in inconsistent inspection outcomes [2]. Therefore, there is a critical need for an automated and vision-based method for counting rebars. Such a method should be capable of evaluating the entire placement rapidly and consistently prior to concrete pouring.

Among vision-based solutions, peak counting in projection profiles remains an actively studied approach. Quek et al. employed a Polynomial-Based Layer Separation (PBLS) algorithm to split inductive-scan images into isolated horizontal and vertical bar layers; the number of bars in each layer was then obtained by locating the peaks in the corresponding one-dimensional projection profiles, although the analyst still had to adjust baseline and threshold settings manually [5]. Park et al. conducted a toy-scale experiment by photographing a rebar mock-up on a site background and stitching the images; after isolating rebar pixels with a Pix2Pix model, they derived the rebar count from peaks in the u/v-axis projection profiles, yet the peaks still had to be selected manually, so full automation was not achieved [2]. Han et al. reconstructed a dense SfM point cloud and projected point density onto an X–Y grid to identify spacing peaks; target-point registration, voxel length, and peak thresholds all required user input, so spacing and rebar counting were not fully automated. [7]. Yuan et al. proposed the SARI algorithm, sliding a 1-D window along each axis of a mobile-LiDAR cloud to detect density peaks and compute spacing; the window length and scan-axis orientation still had to be set by the operator. Hodge & Gattas iteratively sliced a terrestrial-laser point cloud and counted peaks in 2-D density histograms to verify cage geometry, yet window size and occlusion-filter thresholds required manual adjustment [9]. Wu et al. projected TLS point clouds onto principal axes and extracted spacing from histogram peaks; window size, clustering radius, and noise thresholds were dataset-specific settings that inspectors had to choose, leaving user intervention necessary [10]. Song et al. segmented rebars with Rebar-YOLOv8-seg, converted the resulting masks into a 3-D point cloud, and then applied PCA projection followed by RANSAC centre-line fitting to compute rebar spacing; while the algorithm itself needs no user-tuned thresholds, an operator still has to position the camera at an appropriate height and viewing angle, and it also demands a sufficiently large, well-labelled training dataset to maintain segmentation robustness [11].

This paper introduces a parameter-free, two-step framework for fully automated rebar counting. Step 1 converts an orthogonal rebar grid into a concentric-circle pattern by an image-to-polar transformation, so each bar appears as a single circle regardless of camera tilt or in-plane rotation. Step 2 runs a Radial-Transition Voting (RTV)

algorithm that sweeps 360° and selects the mode of black-to-white transition counts, delivering the rebar count automatically. By converting peak counting into circle counting and coupling it with RTV, the framework dispenses with the traditional projection-peak constraints of axis-alignment dependence, noise/occlusion sensitivity, and manual parameter tuning. As a result, it delivers robust, real-time, full-coverage rebar counting from a single greyscale image.

2 Methodology

2-1 Grid-to-Concentric-Circle Transformation

Once a full-coverage site mosaic has been produced, the complex background is removed and only rebar pixels are retained. Rather than treating this as a classical segmentation task, we follow the image-to-image translation strategy of Park et al., a Pix2Pix-GAN and an LSGAN, both trained on synthetically rendered rebar scenes, map the colour photograph to a binary image in which rebar is black and the background white [11].

The black-pixel coordinates (u*, v*) are then normalised to [0, 1] along the horizontal and vertical dimensions, as expressed in Eq. (1).

$$\hat{u} = \frac{u}{W-1}, \qquad \hat{v} = \frac{v}{W-1} \tag{1}$$

Each normalised point is converted to polar space, where the horizontal position becomes the radius and the vertical position the angle. With a one-pixel radial step and a minimum radius d_r and a minimum radius r_{min}= ⌈H/2π⌉, the conversion is given in Eq. (2).

$$r(u) = r_{min} + \hat{u}(\mathrm{W}-1)d_r, \quad \theta(v) = 2\pi\hat{v}, \quad r_{min} = \left\lceil \frac{H}{2\pi} \right\rceil \tag{2}$$

The polar samples are back-projected onto a square canvas of side $2\mathrm{R}_{\max} + 1$ using Eq. (3), where $\mathrm{R}_{\max} = r_{min} + (\mathrm{W}-1)d_r$. Thus an orthogonal rebar grid is re-expressed as m concentric circles—one per bar—independent of camera tilt.

$$x = r\cos\theta + \mathrm{R}_{\max}, \quad y = -r\sin\theta + \mathrm{R}_{\max}, \quad \mathrm{R}_{\max} = r_{min} + (\mathrm{W}-1)d_r \tag{3}$$

Finally, a lightweight morphological post-processing step—closing followed by optional skeletonisation—bridges small threshold gaps and thins each circle to a stable one-pixel contour. Because these operations use fixed, task-independent settings, no additional parameters are introduced. By reformulating the peak-counting problem into a circle-counting problem in this way, the proposed approach eliminates axis-alignment, noise/occlusion, and manual-tuning issues that hinder projection-profile techniques.

2-2 Radial-Transition Voting (RTV)

After the concentric-circle image I_c has been formed, the number of rebars is obtained by a two-step radial-transition voting procedure.

First, a user-selectable set of N unit vectors is cast from the image centre. If the default value N=360 is used, the i-th ray makes an angle of $2\pi i/N$ radians with the positive x-axis, as introduced in Equation (4).

$$\theta_i = \frac{2\pi i}{N}, \quad i = 0, \dots, N-1 \tag{4}$$

Along each ray, the algorithm starts just outside the inner skip band $r_{min} + \delta$ and marches outward to the outer radius $\mathrm{R_{max}}$. Whenever a black pixel (rebar) is immediately followed by a white pixel (background), one black-to-white transition is counted. The total number of such transitions on the i-th ray is denoted T_i and defined formally in Equation (5), where $I(r, \theta_i)$ returns the binary value of I_c at polar position (r, θ).

$$T_i = \sum_{r_{min}+\delta}^{R_{max}} [I(r, \theta_i) = 1 \wedge \mathrm{I(r-1}, \theta_i) = 0] \tag{5}$$

Finally, the histogram of all T_i values collected from all N rays is analysed. The mode—i.e. the transition count that occurs most frequently—is selected as the rebar number m. Let $\mathcal{K} \subset \mathbb{N}_0$ be the set of candidate counts. Then the rebar number is determined by majority voting, where $1(\cdot)$ is the indicator function. This process is formalized in Equation (6).

$$m = \underset{k \in \mathcal{K}}{argmax} \sum_{\mathrm{i=1}}^{N} 1(T_i = k) \tag{6}$$

Because genuine concentric circles generate exactly the same transition count on almost every ray, whereas noise and local gaps yield scattered counts, RTV suppresses false detections without any user-defined thresholds, bandwidths, or window size.

3 Implementation

This section verifies whether the proposed Cartesian-to-polar transformation followed by Radial-Transition Voting (RTV) can count rebars with high precision in a fully automated setting while all parameters remain fixed. The validation begins with greyscale binary images produced by the image-to-image translation pipeline of Park et al. [11]; that network suppresses background noise and converts every rebar pixel to black against a white background, eliminating any need for manual threshold tuning.

Figure 3-1 presents the two test images, with image (b) obtained by rotating image (a) through 90 degrees. Because the counting algorithm focuses on vertical reinforcement, rotating the image by 90 degrees makes it possible to count the previously horizontal rebars as well. Both images include a slight in-plane tilt and small surface blemishes to mimic realistic field conditions.

Throughout the study every hyper-parameter is held constant. The polar grid is sampled along 360 radial directions at one-degree intervals; the radial step is fixed at one pixel, and all pixels within a radius of ten pixels from the centre are excluded to suppress centre-finding noise. Morphological closing is implemented as one dilation–erosion pair repeated six times. These settings belong intrinsically to the method and remained unchanged throughout all experiments.

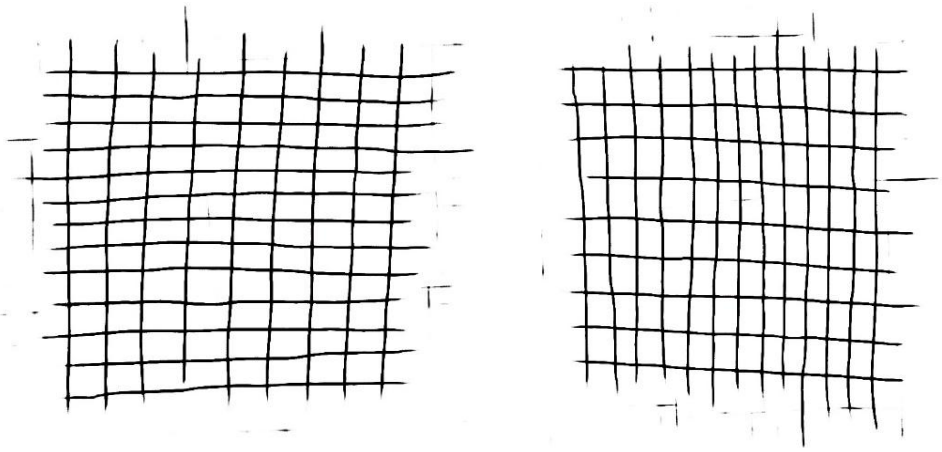

Figure 3-1: Greyscale binary validation images: (a) original orientation; (b) image rotated through 90 degrees.

For baseline comparison the same images were processed with the conventional projection-profile technique, and the resulting histograms are shown in Figure 3-2. The profiles expose two chronic weaknesses. First, when glare or speckle noise breaks a bar contour, the single intensity peak that should represent one bar splits into several smaller peaks, so reliable counting becomes impossible without human supervision. Second, peak height and width vary with camera distance and image resolution, forcing analysts to recalibrate smoothing strength and threshold values for every project. Because of these limitations, projection profiles cannot deliver fully unattended rebar counts.

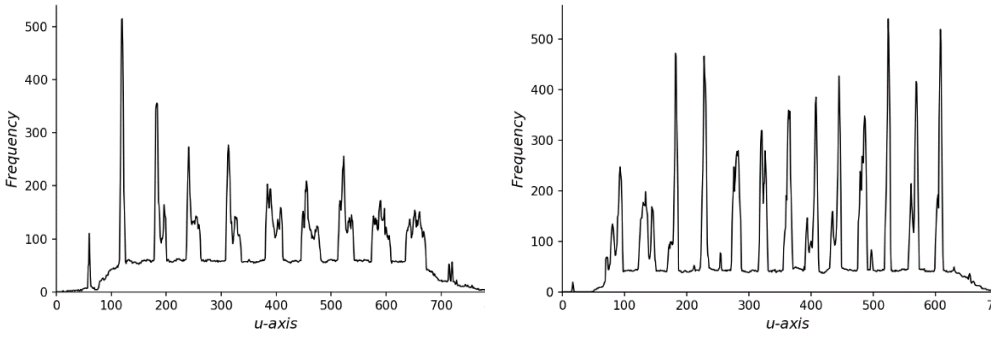

Figure 3-2: Projection-profile histograms obtained from the images in Figure 3-1; the multiplicity and irregularity of peaks illustrate the method's sensitivity to noise, tilt and parameter choices.

The proposed pipeline avoids these pitfalls by mapping each Cartesian pixel (u, v) to polar coordinates $(r, \theta) = (u, 2\pi v)$. After transformation every vertical bar becomes a single continuous concentric circle, whereas horizontal bars appear as radial lines and therefore do not interfere with circle counting. RTV then emits 360 uniformly spaced rays, discards the central ten-pixel core, and records the number of black-to-white transitions along each ray. The statistical mode of the 360 transition counts is taken as the final estimate of the number of rebars; because spurious transitions caused by blemishes or partial occlusions affect only a few rays, the modal vote is robust to noise.

Figure 3-3 visualises the transformed images. In Figure 3-3a nine distinct circles correspond exactly to the nine vertical bars in the original view; Figure 3-3b shows thirteen circles that match the thirteen bars now oriented vertically after rotation. The circles remain sharply separated despite slight bar inclinations and scattered noise, confirming the resilience of the polar representation.

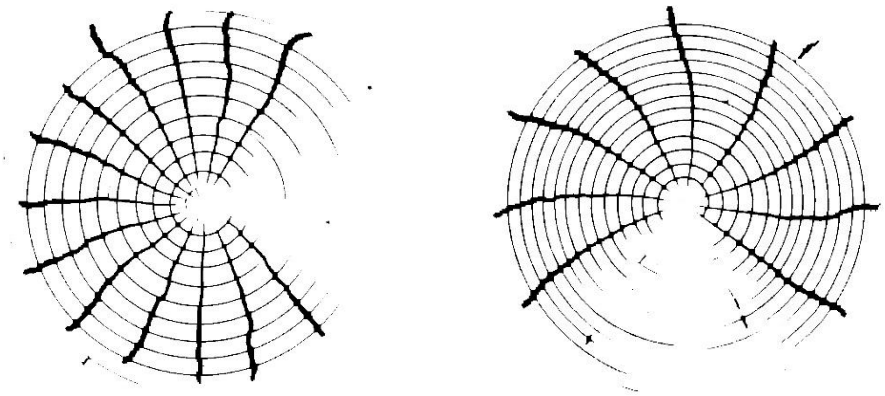

Figure 3-3: Results of the Cartesian-to-polar transformation: (a) nine concentric circles derived from Figure 3-1a; (b) thirteen concentric circles derived from Figure 3-1b.

Quantitative results in Table 3-1 demonstrate that RTV reproduces the ground-truth counts without error for both images. Moreover, Table 3-2 shows that the modal transition count attracts more than one-third of all rays—122 out of 360 in the first image and 153 in the second—while every alternative receives far fewer votes. Such a decisive majority indicates that random noise and minor contour breaks exert negligible influence on the final decision.

In summary, by reformulating rebar counting as circle detection and replacing hand-tuned thresholds with a data-driven voting scheme, the Cartesian-to-polar transformation combined with RTV attains 100 % accuracy under realistic photographic conditions using a single, immutable parameter set, thereby

overcoming the obstacles that prevent full automation in projection-profile approaches.

Image	Ground-truth rebars	RTV estimate	Modal votes (out of 360)	Coverage (%)
Original orientation	9	9	122	34
90° rotated	13	13	153	43

Table 3-1: Accuracy of RTV-based rebar counting for the two validation images.

Rank	Transition count	Rays (votes)	Vote Share (%)
1	9	122	33.9
2	10	61	16.9
3	0	25	6.9
4	1	24	6.7
5	8	21	5.8

Table 3-2a: Five most common radial transition counts recorded by RTV; (a) Original orientation (Fig. 3-3a)

Rank	Transition count	Rays (votes)	Vote Share (%)
1	13	153	42.5
2	12	34	9.4
3	11	24	6.7
4	1	24	6.7
5	2	16	4.4

Table 3-2b: Five most common radial transition counts recorded by RTV; 90° rotated (Fig. 3-3b)

5 Conclusions

The proposed Cartesian-to-polar transformation pipeline combined with Radial-Transition Voting (RTV) removes the long-standing obstacles to full automation in rebar inspection—mandatory axis alignment and manual threshold adjustment. A proof-of-concept evaluation used two challenging images, one in its original orientation and the same frame rotated 90 degrees, to test the method with a single fixed parameter set. In both cases the pipeline exactly matched the ground-truth counts and secured a dominant vote share greater than one third of all 360 rays. These findings show that the system achieves push-button accuracy where classical projection-profile techniques break down. Future research will assemble a large-scale public dataset covering diverse lighting conditions, camera angles, and bar spacings

to provide rigorous benchmarks and uncover edge cases. An equally important direction is to extend the current two-dimensional approach so that it can count rebars in multi-layer cages and fully three-dimensional arrangements encountered on actual sites. Together, these efforts aim to create a universally applicable, high-confidence tool that delivers real-time automated rebar auditing across diverse construction scenarios.

Acknowledgements

This work was supported by the National Research Foundation of Korea (NRF) grant funded by the Korea government Ministry of Science (No. 2021R1A2C3008989).

References

[1] B.F. Spencer Jr., V. Hoskere, Y. Narazaki, "Advances in computer-vision-based civil infrastructure inspection and monitoring", Engineering, 5 (2), 199-222, 2019, DOI:10.1016/j.eng.2018.11.030.

[2] J.-S. Park, S.-T. Chun, S.-K. Hong, "A Preliminary Study on the Automation of Rebar Placement Inspection at Construction Sites", KOREAN SOCIETY ADVANCED COMPOSITE STRUCTURES, 16 (1), 28-37, 2024, DOI:10.12652/KSCM.2024.16.1.028.

[3] H.-W. Hsu, S.-H. Hsieh, "Applying augmented-reality technique to support on-site rebar inspection", Proceedings of ISARC 2019, 1004-1011, 2019, DOI:10.22260/ISARC2019/0138.

[4] H.-L. Chi, M.-K. Kim, K.-Z. Liu, J.P. Thedja, J. Seo, D.-E. Lee, "Rebar inspection integrating augmented reality and laser scanning", Automation in Construction, 136, 104183, 2022, DOI:10.1016/j.autcon.2022.104183.

[5] S. Quek, P. Gaydecki, B. Fernandes, G. Miller, "Multiple layer separation and visualisation of inductively scanned images of reinforcing bars in concrete using a polynomial-based separation algorithm", NDT & E International, 35 (4), 233-240, 2002, DOI:10.1016/S0963-8695(01)00053-3.

[6] K. Han, J. Gwak, M. Golparvar-Fard, K. Saidi, G. Cheok, M. Franaszek, R. Lipman, "Vision-based field inspection of concrete reinforcing bars", Proceedings of ICCVR 2013, 105-112, 2013, DOI:N/A.

[7] X.X. Yuan, A. Smith, R. Sarlo, C.D. Lippitt, F. Moreu, "Automatic evaluation of rebar spacing using LiDAR data", Automation in Construction, 131, 103890, 2021, DOI:10.1016/j.autcon.2021.103890.

[8] T. Hodge, J. Gattas, "Geometric and semantic point cloud data for quality control of bridge girder reinforcement cages", Data in Brief, 45, 108742, 2022, DOI:10.1016/j.dib.2022.108742.

[9] H. Wu, A. Al-Habaibeh, R. Irvine, "Laser scanning point cloud-based inspection system for reinforcement elements in precast concrete construction", Automation in Construction, 150, 104858, 2023, DOI:10.1016/j.autcon.2023.104858.

[10] [11] M. Song, D. Kim, J. Kim, "A deep-learning-based rebar detection framework using RGB-D camera and YOLOv8-seg model for point cloud-

based spatial analysis", KSCE Journal of Civil Engineering, In Press, 2025, DOI:N/A.
[11] J.S. Park, H.S. Park, "Automated reconstruction model of a cross-sectional drawing from stereo photographs based on deep learning", Computer-Aided Civil and Infrastructure Engineering, 39(3), 383–405, 2024, DOI:10.1111/mice.13071.